PROCEEDINGS, 49th Workshop on Geothermal Reservoir Engineering
Stanford University, Stanford, California, February 12-14, 2024
SGP-TR-227

Application of low temperature thermochronology for exploration of blind geothermal systems: A case study from the Kigluaik fault system and Pilgrim Hot Springs, northwestern Alaska

Jason W. Craig,[1] Elizabeth L. Miller,[1] Jeff A. Benowitz,[2] Max Manson,[1] Trevor A. Dumitru[1], and Carl W. Hoiland[3]

1. Department of Earth and Planetary Sciences, Stanford University, Stanford, CA 94305-2115

2. GeoSep Services, Moscow, Idaho 83843

3. Zanskar Geothermal & Minerals, Inc., Salt Lake City, UT 84101

Communicating author: jwcraig@stanford.edu

Keywords: Alaska, Seward Peninsula, Nome, geothermal, structure, exploration, fault, thermochronology

ABSTRACT

Development of geothermal resources would provide reliable baseload power to isolated communities of the Seward Peninsula that currently depend on fossil fuels for energy. Pilgrim Hot Springs (PHS) has been the main geothermal exploration focus in the region, but multiple drilling efforts have not yet successfully targeted the geothermal system. The Kigluaik Mountains lie ~ 5 km south of PHS and are bound by an active normal fault system that has not been assessed as a structural control for geothermal upwelling. This study evaluates the relationship between the Kigluaik fault system (KFS) and PHS through the application of low temperature thermochronology from samples collected along the KFS trace and drill core from geothermal wells at PHS. Thermochronology from rocks collected from the exposed footwall of normal fault systems is a novel and cost-effective approach for discovering areas with blind hydrothermal activity. Samples along the KFS largely yield 40-25 Ma apatite (U-Th)/He (AHe) dates, with two samples yielding anonymously young average (13 Ma) dates. Two samples from drill core sampled directly in the KFS damage zone produced young single AHe grain dates of 9, 6, and 4 Ma. Areas with young AHe dates indicate zones with potential (active or fossil) blind geothermal systems and are considered future exploration targets. Thermochronology results do not indicate that PHS is directly controlled by the KFS. A concealed fault within the basin at a high angle to the KFS is likely the primary structure controlling upflow at PHS. AHe results from drill core in the zone of outflow at PHS are similar to young samples from the KFS and yield anomalously young single-grain ages that range from 13-0.5 Ma. GeoT multicomponent geothermometry estimates indicate 137°C reservoir temperatures for PHS and confirm prior estimates that the region contains moderate temperature geothermal systems that could be economic sources of renewable power once successfully targeted.

1. INTRODUCTION

Nome is an isolated community of ~3,700 people that is located on the southwestern edge of the Seward Peninsula, western Alaska (Fig. 1). The residents of Nome, like much of the rest of rural Alaska, rely on diesel-burning generators. The associated cost of energy in this community is substantially greater (>$7 per gallon of diesel) than the national average, caused largely by the high costs of fuel transportation. The development of reliable and affordable energy in this region is vital to sustain basic infrastructure and avoid fuel cost related community economic decline (Berman, 2017), but there are currently limited options for energy in rural Alaska that are not sourced from fossil fuels. Utilization of a geothermal resource on the Seward Peninsula would provide reliable baseload power to the region with a reduced environmental impact. Reevaluation of the geothermal potential of the Seward Peninsula using structurally focused exploration strategies may provide a new perspective for characterizing the geothermal resources.

Pilgrim Hot Springs (PHS) is located ~ 5 km north of the Kigluaik Mountains (Fig. 1) and ~60 km north of Nome. The surface expression of PHS includes a series of hot pools (60-75˚C), anomalous vegetation, and lack of permafrost that stands in stark contrast with the surrounding landscape (Haselwimmer et al., 2013). The geologic controls for PHS have been proposed to be related to radiogenic heat produced by Cretaceous plutons (Kolker, 2008), Quaternary magmatism (Westcott and Turner, 1981; Motyka et al., 1980), or amagmatic fault-controlled hydrothermal circulation (Turner and Swanson, 1981; Glen et al., 2014; e.g. Curewitz and Karson, 1997). The geothermal fluids are saline alkali-chloride springs which are consistent with a magmatic fluid source; yet a $^{3}He/^{4}He$ ratio of 0.9 (R/R_{atm}) is below values for most geothermal systems that are directly related to magmatism, which indicates a component of mantle derived helium gas (Liss and Motyka, 1994; Rizzo et al., 2022). The stable isotope composition of the thermal water at PHS is almost the same as the Pilgrim River, indicating the river is the major source of recharge to the thermal aquifer (Liss and Motyka, 1994). Classical geothermometry estimates of a ~150˚C reservoir for PHS (Miller et al., 1973; Lofgren, 1983; Liss and Motyka, 1994) instigated drilling campaigns in the early 1980's to exploit the geothermal resource. Maximum temperatures encountered by drill holes were only 91˚C from a shallow reservoir (Kunze and Lofgren, 1983; Lofgren, 1983) and not adequate for economic production. Exploration resumed in 2010 with numerous detailed studies that culminated in drilling new wells (ACEP, 2015). Temperature reversals were ubiquitous across the well field and the same maximum temperature of 91°C (Benoit et al., 2014a, 2014b) ultimately proved that drilling had not successfully targeted the source of upwelling.

This study evaluates conceptual models of the PHS geothermal system by integrating Quaternary mapping, structural analysis, and aqueous geothermometry with low temperature thermochronology (Reiners et al., 2005) to identify structurally controlled zones of

hydrothermal upflow. At least two conceptual models exist for the upflow of hydrothermal fluids at PHS: A) blind faults within the Imuruk basin (e.g., Glen et al., 2014; Benoit, 2014a, 2014b; Miller et al., 2013a, 2013b), and B) the active Kigluaik normal fault. We used low temperature thermochronology along the trace of the Kigluaik fault system to investigate thermochronology as a tool for geothermal exploration of fault-controlled blind geothermal activity. The integrated approach employed in this study tests conceptual models of PHS and identifies regional targets for future geothermal exploration programs.

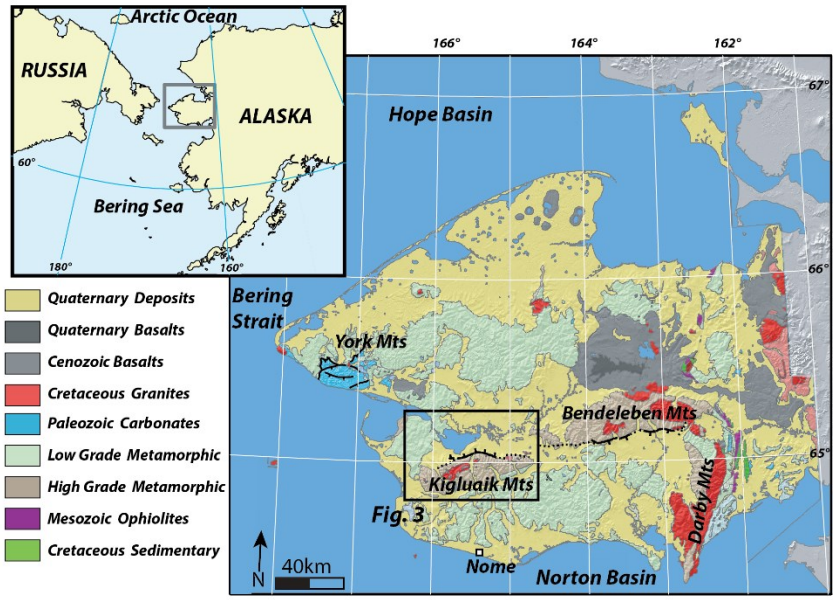

Figure 1: Location and simplified bedrock geologic map of the Seward Peninsula after Till et al. (2011) and modified from McDannell et al. (2014). The location of the map extent shown in Figure 3 is the labeled black rectangle.

The use of high-resolution thermochronology from rocks along the surface trace of normal faults is a novel approach for attempting to locate zones of blind hydrothermal activity. The apatite fission track (AFT) and zircon (U-Th)/He (Zhe) systems generally record temperatures of around 120°C and 180°C, respectively (e.g., Flowers et al., 2022a; Donelick et al., 2005), and are used in this study as background temperature constraints. The apatite (U-Th)/He (AHe) system is sensitive to lower-temperature thermal disturbances in the 60-80°C range (e.g. Farley, 2000) and has been observed to display partially or fully reset ages related to circulating hydrothermal fluids in fault zones (Berger et al., 2022; Louis et al., 2019; Milesi et al., 2019; MacNamee, 2015; Gorynski et al., 2014). Use of low temperature thermochronology as a geothermal exploration tool provides a low-cost, minimally invasive technique to test a normal fault system for the presence of geothermal activity (e.g. Fig. 2).

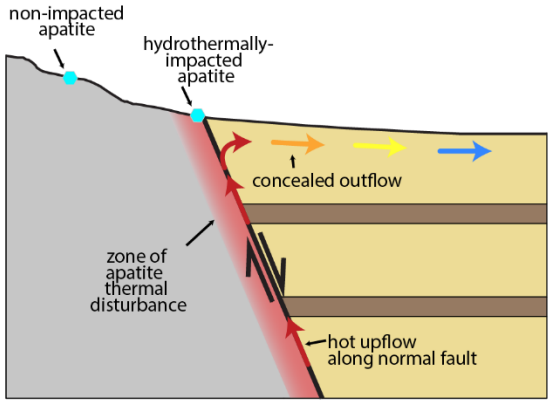

Figure 2: Schematic model for a blind geothermal system and sampling strategy in rocks adjacent to a recently active normal fault to detect hydrothermally impacted partially reset apatite using (U-Th)/He thermochronology. Higher temperatures could lead to fully reset apatite (U-Th)/He dates. AHe signal of hydrothermally impacted apatite in the figure assumes that the fault has exhumed the footwall sample after heating from direct contact with hydrothermal fluids has occurred. Figure modified from Richards and Blackwell (2002).

The Kigluaik Mountains of the Seward Peninsula (Figs. 1 and 3) are a gneiss dome that initially developed during mid-Cretaceous extension (Amato and Miller, 2002; Amato et al., 1994; Miller et al., 1992). Although the gneiss dome mostly cooled during the latest Cretaceous to early Cenozoic based on $^{40}Ar/^{39}Ar$ thermochronology and apatite fission track data (Dumitru et al., 1995; Calvert et al., 1999), it is bound on its northern side by the active Kigluaik normal fault system (KFS) (Fig. 3), which displaces Quaternary glacial deposits in many places along its trace (Hudson and Plafker, 1978)(Fig. 3). The relation of the KFS to other Quaternary features and to the tectonic setting of Seward Peninsula and the Bering Strait region is presented in Miller and Craig (this volume). The KFS is one of the main extensional fault systems in the region and separates the northern range front of the Kigluaik Mountains from the Imuruk Basin (Fig. 3 and 6b).

2. METHODS AND RESULTS

We employ Quaternary mapping, structural analysis, fluid geochemistry investigations, and thermochronology to evaluate areas of potential upwelling hydrothermal fluids along the KFS. These methods are used to assess the nature of known hot springs, structural controls, and areas with possible blind geothermal activity in the region.

2.1 Quaternary mapping

A high-resolution digital elevation model (DEM) was produced from 50 cm areal photogrammetry collected for this study and combined with the 2-m Arctic DEM (Porter et al., 2022) and LiDAR data (Dannen, pers. commun.) to map the KFS (Fig. 3). The KFS is a north-dipping, generally east-west striking, ~ 80 km-long normal fault system. Recent fault scarps range in height from 4-10 m as measured by offsets of Quaternary units (Hudson and Plafker, 1978) to greater than 60 m in recently offset bedrock adjacent to the fault (Fig. 6b). Quaternary units with mapped fault scarps include alluvial fans and glacial moraines associated with the last glacial maximum (27-12.5 ka) (Tulenko et al., 2022; Young et al., 2019, Briner et al, 2017; Hamilton et al., 1986; Kaufman et al., 1986).

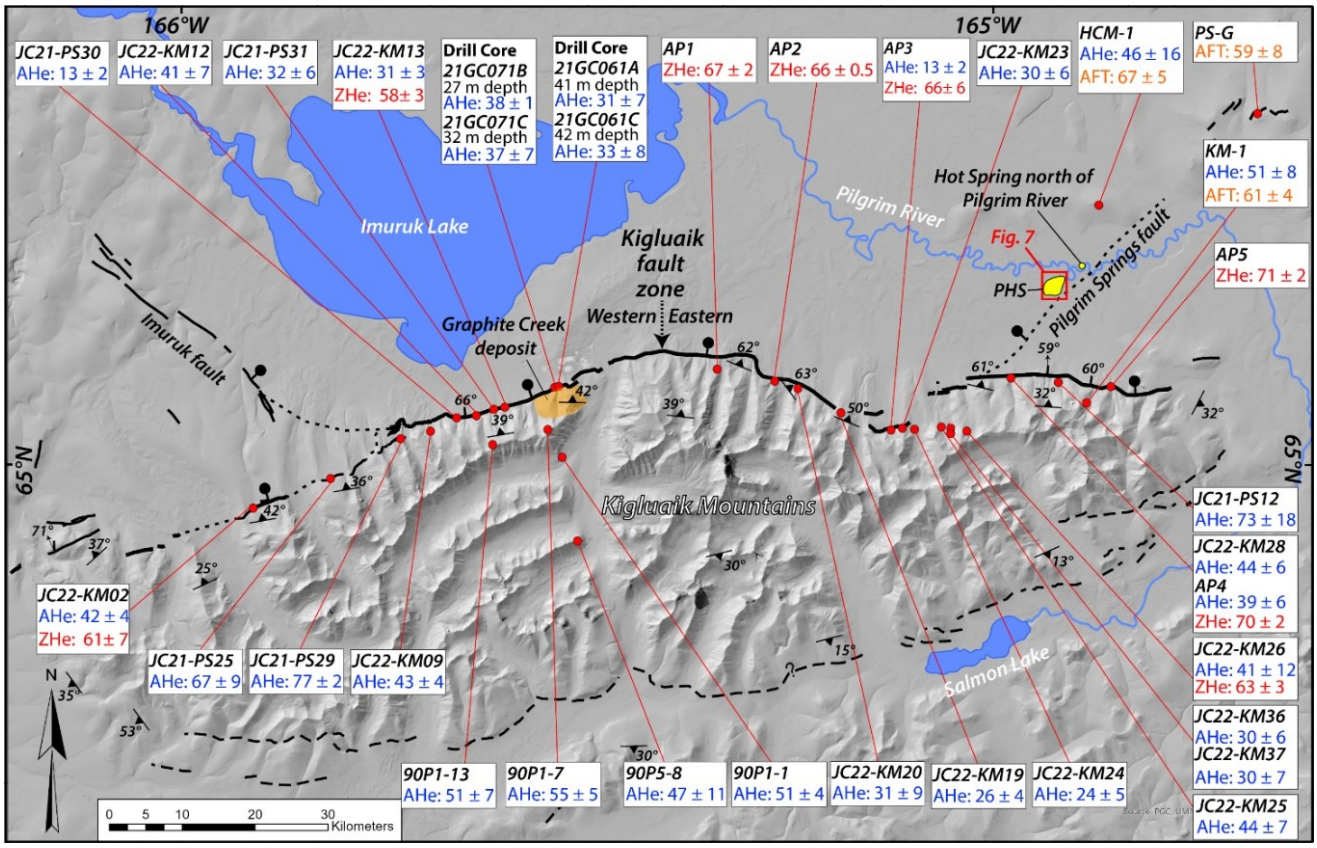

Figure 3: Map of the Kigluaik Mountains and Pilgrim Hot Springs study area (location shown in Fig. 1). Mapped Quaternary fault scarps are black lines with ball on downthrown side. Location and extent of Pilgrim Hot Springs and unnamed hot springs north of the Pilgrim River (Daanen, pers. commun.) are shown in yellow. Location of the Graphite Creek deposit shown in orange. Location of thermochronology samples shown as red dots with (U-Th)/He zircon (ZHe; red), apatite fission track (AFT; orange), and apatite (U-Th)/He (AHe; blue) sample average cooling ages displayed below sample names (at top of lists). Structural data collected in this study supplemented by measurements from Amato and Miller (2004). Western and eastern portions of the KFS separated by dashed black arrow and referenced in text. Queried fault along southern side of mountain range after (Koehler and Carver, 2018), as mapped geologically, no offset on this fault (Amato and Miller, 2004).

The KFS contains two mapped segments that are separated near the Cobblestone glacial valley. The western segment is a discrete ENE-WSW-striking fault scarp that bounds the greatest gradient in topography south of Imuruk Lake. The eastern segment is a series of discontinuous E-W to WNW-ESE striking-scarps separated by step-overs. The Imuruk fault is a NW-SE striking fault bounding the western Imuruk Basin and intersects the KFS in the western segment near sample JC21-PS30 (Fig. 3). A concealed NE-SW striking fault directly south and adjacent to the surface manifestations of PHS (Glenn et al., 2014), referred to as the Pilgrim Springs fault in Fig. 4, intersects the eastern segment of the KFS.

The KFS does not displace the last glacial maximum deposits everywhere, indicating that some recent displacement occurred prior to ~15-12.5 ka. The western portion of the range-bounding fault has not been modified by Quaternary glaciation, whereas the eastern segment has been extensively modified. To the west, the trace of the KFS dies off and is covered by colluvium. To the east, the KFS takes a series of northern steps and does not overlap with the south dipping Bendeleben normal fault system (Fig. 1) (Hudson and Plafker, 1978; McDannell et al., 2014).

2.2 Structural analysis

Structural analysis was completed on rock fabrics measured in outcrop along the KFS and oriented drill core from the Graphite Creek deposit (Figs. 3, 4 and 6). Structural data were projected onto equal area lower hemisphere projections (Fig. 4). Fault planes in outcrop along the range front generally dip steeply (~50-60°) to the north and slickenlines indicate normal-slip kinematics (Fig. 4a). Exposures of high-quality fault surfaces were limited due to frost heaving and glacial reworking. Metamorphic foliation in footwall rocks dips moderately to steeply (33-77°) north and generally has strike-perpendicular N-S stretching lineations (Fig. 4b).

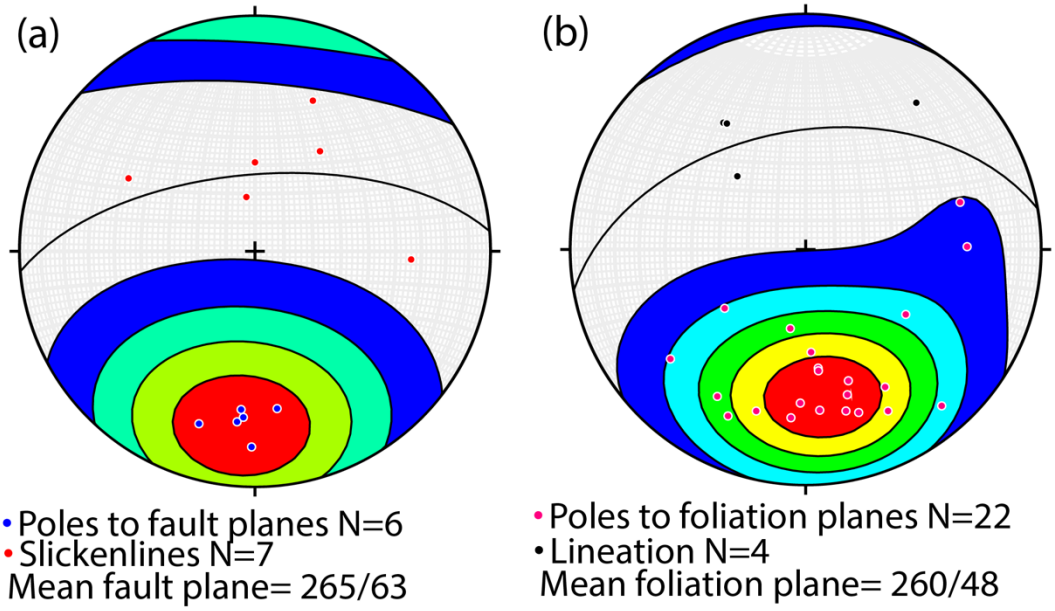

Figure 4: Equal area stereonet projections of structural measurements taken from footwall outcrop exposures of the KFS. (a) Contoured fault poles (blue dots) and slickenlines (red dots). (b) Metamorphic foliation (contoured pink dots) and lineation (black dots). Stereonets generated using Stereonet v. 11.3.1 software (Allmendinger et al., 2012; Cardozo and Allmendinger, 2013).

Location and elevation of the subsurface Kigluaik fault plane was measured in seven oriented drill holes (locations omitted for proprietary reasons) taken from the Graphite Creek deposit (near samples 21GC061 and 22GC071 in Fig. 3). These data were used with the mapped surface fault scarp to generate three-point problem estimates of the local orientation and dip of the KFS (Table 1). The calculated strike for the local orientation of the fault ranges from 064-083 degrees AZ and dips range from 25-65°, with an average geometry of 072/47° NW. There is some uncertainty in three-point problem fault dip values based on the position of the mapped fault scarp due to erosion and the relatively short depth interval to the fault in drill core.

Table 1: Fault geometry data from oriented drill core at Graphite Creek mineral deposit. Location of drill holes 21GC062 and 22GC071 shown in figure 3.

Drill Hole	Calculated fault strike (AZ)	Calculated fault dip (degree)
18GC023	064	42
18GC024	070	65
18GC025	083	60
18GC026	070	57
21GC061	064	31
21GC062	074	52
22GC071	076	25

2.3 Fluid geochemistry investigations

Five new water samples were collected for this study in the summer of 2021 (Table 2). Water samples were collected from a natural hot spring at PHS, wells PS13-1 and PS13-3, one sample from the Pilgrim River, and one sample from a creek in the Kigluaik Mountains. Preliminary GeoT multicomponent equilibria analysis (Spycher et al., 2014) was completed on one legacy water sample of well PS-2 (1979 analysis in Table 2; Liss and Motyka, 1994) which yielded a ~136.5 ± 5°C geothermometer estimate (Fig. 5) (N. Spycher, pers. commun.). Classical geothermometry estimates completed in this study from sample PS-2 range from 136-170°C.

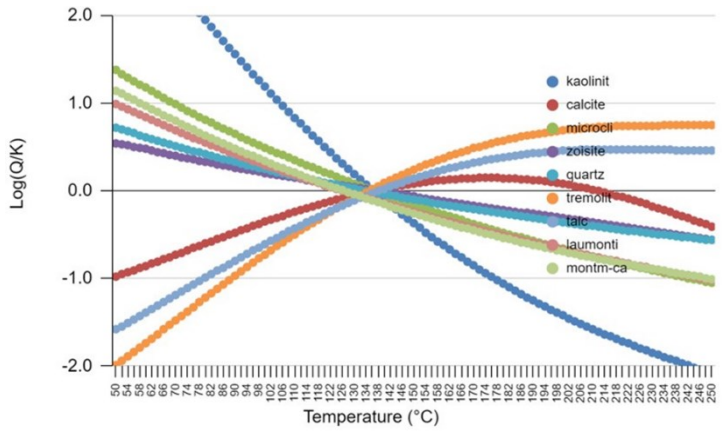

Figure 5: GeoT multicomponent chemical equilibria model results. The selected minerals attain equilibria under the modeled conditions for well PS2 from legacy 1979 water chemistry data at 136.5 ± 5°C.

Table 2: Pilgrim Hot Springs water chemistry. All data prior to 2021 are from ACEP (2015) PHS final report. Values in ppm. ND= not determined.

Sample	Date	T	pH	Na	K	Ca	Mg	Li	B	Si02	HC03	C03	S04	Cl	F
--	--	°C	--	ppm	ppm	ppm	ppm	ppm	ppm	ppm	ppm	ppm	ppm	ppm	ppm
Spring (hot)	2021	60	6.94	1370	61.4	511	ND	3.92	2.14	65.4	17.6		ND	3380	5.6
PS13-1	2021	74.9	7.8	890	47.4	335	ND	2.46	ND	61.1	26.6		ND	2100	3.9
PS13-3	2021	77.2	7.5	872	42.2	324	ND	2.41	ND	61	22.5		ND	2090	3.9
PS13-3	2021	77.2	7.2	882	43.1	324	ND	2.49	ND	61.7	21.6		ND	2090	3.4

River (cold)	2021	8	7.56	ND	ND	40.6	ND	ND	ND	ND	73.3		69.3	2.44	ND
Spring (cold)	2021	1.7	6.81	ND	ND	10.6	ND	ND	ND	ND	21.6		11.4	ND	ND
Spring (hot)	1915	70		1590	61	545	7.4			87	21		25	3450	
Spring (hot)	1972	82	6.75	1450	61	530	1.4	4	2.4	100	30.1		24	3346	4.7
Spring (hot)	1982	55	6.8	1660	59	542	1	4.5	2.2	91	36		15	3360	4.3
Spring (hot)	1993	42	6.5	1580	65	569	1.5	4	2.7	86	19		18	3530	4.7
Spring (hot)	1993	55	6.8	1660	59	542	1	4.5	2.2	91	36		15	3360	4.3
Spring (hot)	2012		6.65	1480	62.8	508	0.38	3.6	2	86	14		22	3350	4.6
Spring (hot)	2014	73	6.63	1400	58	460	1	3.4	2.1	80	15			3500	
PS-1	1979	90.5	6.4	1828	75	518	0.9	3.9	2.5	95	16		16	3590	4.8
PS-1	1982	92	7.5	1720	60	511	0.9	4.7	2.3	94	30		19	3420	4.4
PS-1	1993	82	7.1	1560	65	545	0.6	4.2	2.4	90	20		7	3460	5.3
PS-1	2010	79	7.1	1530	61.6	519	1.21	3.5	2.2	83	27.8		14.3	3460	4.5
PS-2	1979	90	6.4	1820	75	516	0.9	3.9	2.3	101	19		15	3540	4.8
PS-2	1982	96	7.3	1510	57	516	0.9	4.7	2.3	92	26		19	3420	4.5
PS-3	1982	75	8	592	25	260	0.4	2	1	60	36		15	1430	1.3
PS-3	1993	65	6.8	1100	43	441	0.6	3.2	1.5	67	27		6	2450	2.9
PS-3	2010	67	7	1140	40.9	412	0.85	2.8	1.7	71	23.7		10.8	2650	3
PS-4	1982	48	8.6	115	4.8	23	0	0.3	0.5	35	80		11	284	0.5
PS-4	1993	45	8.6	146	7.8	98	0.2	0.2	0.2	27	48		1	386	0.3
PS-4	2010	44	8.52	152	5.9	73	0.14	0.5		28	34		9.4	353	0.4
PS-4	2013	44.6	8.47	128	5.5	45	0	0.4	0.2	29	39.9	1.5	9.3	260	0.6
PS-5	1993	32	9.6	36	1.1	2	0.2	0.1	0.6	21	81		5	6	0.5
PS-5	2010	30	9.6	36	1.09	1	0	0.1		20	49.6		5.4	2	0.5
Ml-1	1982	22	9.7	16	0.5	5	0	0.1		21	37		9	5	0.2
Ml-1	1993	31	8.3	29	1.5	23	0.6	0.2	0.1	20	32		10	66	0.2
Ml-1	2010	29	7.8	130	4.4	93	0	0.5		21	25.8		9.5	337	0.2
PS 12-3	2012	65.5	7.52	731	29.9	281	0.78	1.8	1	51	30.6		8.2	1640	1.9
PS 13-1 (open to 1036ft)	2013	70.5	7.51	537	26.1	236	0.4	1.4	0.8	54	25.1		9.3	1300	1.4
PS13-1 (shallow completion)	2013	77	7.27	1090	50.9	370	0.7	2.6	1.5	79	22.8		12.4	2500	3.3
PS 13-1300gpm	2014	79	7.26	1000	35	250		2	1.5	59	18			2500	
PS 13-160gpm	2014	77	7.05	950	37	250		2.1	1.4	67	15			2300	
PS 13-2	2013	71	8.95	124	25	49	0	0.3	0.2	62	39.4	11.1	5.8	265	0.5
PS 13-2 55 gpm	2014	69	7.52	53	3.1	9		0.2	0.1	54	62		5.5	65	
PS 13-3	2013	79	7.27	1070	46.3	373	0.7	2.5	1.4	74	22.1		12.3	2424	3
PS 13-3 60gpm	2014	78	6.97	920	37	280		2.2	1.3	66	16			2200	

2.4 Thermochronology

Samples were collected from KFS fault plane exposures and drill core sourced from the Graphite Creek deposit and PHS geothermal wells (Figs. 3, 6, and 7). Multiple thermochronology methods were used with a range of closure temperatures from ~ 220˚C to 60˚C. We mainly focused on apatite (U-Th)/He (AHe) dating (39 samples total) to identify anomalously young cooling dates that may be associated with zones of geothermal upwelling. For select samples, multiple minerals were dated to provide greater insight into the cumulative thermal history. Zircon (U-Th)/He (ZHe) dates were used to constrain the upper end of the low-temperature history as zircon will generally experience complete loss of radiogenic helium at temperatures greater than 220°C and partial retention of helium down to ~180°C for rapidly cooled samples with minimum radiation damage (Guenthner et al., 2013; Ginster et al., 2019). Depending upon radiation damage and other factors, the ZHe closure temperature can vary substantially and be as low as 50°C (Johnson et al., 2017). Apatite fission track (AFT) analyses were used as an intermediate thermochronometer between Zhe and AHe, as this technique is sensitive to cooling histories between 120°C and 60°C (Tagami and O'Sullivan, 2005). Sample locations and dates are presented in Figures 3 and 7.

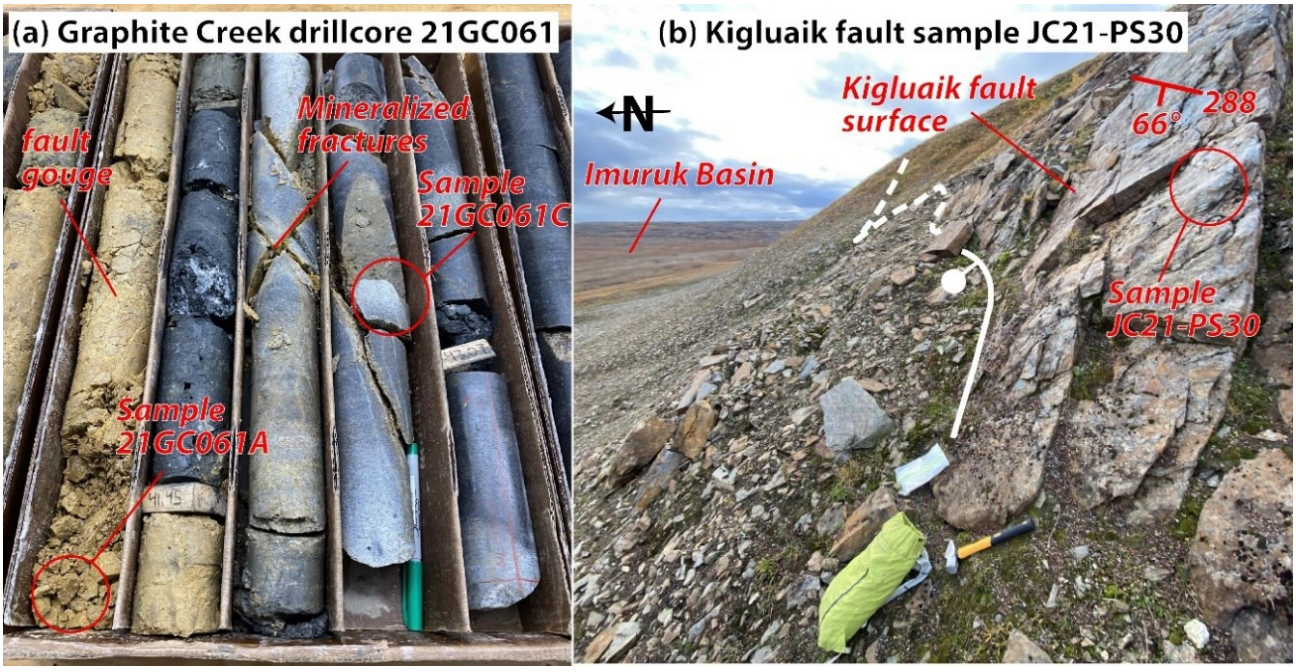

Figure 6: Photographs of KFS samples used for (U-Th)/He thermochronology. Sample localities shown in Figure 3. (a) Graphite Creek drill core 21GC061 with annotated sample locations, fault gouge, and mineralized fractures. Sharpie (14 cm) for scale. (b) Outcrop along KFS scarp at sample JC21-PS30 (looking east). Hammer (30 cm) for scale.

Zircon and apatite (U-Th)/He data were produced at the University of Colorado Thermochronology Research and Instrumentation Laboratory (CU TRaIL) and follow conventions for processing and interpreting (U-Th)/He data outlined in Flowers et al. (2022a, 2022b). Apatite fission track analyses were completed at the GeoSep Services facilities in Moscow, Idaho, USA, using methods described in Donelick et al. (2005).

ZHe average cooling ages from samples collected from bedrock outcrops along the KFS range from Late Cretaceous to Paleocene (71 to 58 Ma) (Fig. 3). Pooled AFT ages from bedrock and detrital samples composed of indurated sediments of intermixed silts, sands, and gravels from wells at PHS (e.g. Miller et al., 2013a and 2013b) vary from 67 to 59 Ma (Figs. 3 and 7). AHe average dates from samples collected from bedrock outcrops along the KFS range from 73 to 13 Ma, with most samples yielding Paleocene to late Oligocene ages (50 to 25 Ma). The ZHe and AHe dates shown in Figure 3 are the average of individual selected grain dates from the sample; uncertainty is the standard deviation of the range of individual dates in a sample. The youngest sample average AHe dates in are samples Ap3 (N=2) and JC21-PS30 (N=9), both yielding 13 Ma dates. AHe dates are generally older along the eastern and western ends of the KFS and younger toward the center of the fault. AHe dates also increase with elevation and distance to the south from the KFS.

Four samples of faulted rock and fault gouge intercepted in two drill holes at the Graphite Creek deposit (samples 21GC061 and 21GC071; Figs. 3 and 6) were processed for AHe. These samples yield Eocene-Oligocene average AHe dates similar to those in outcrop samples. Despite numerous grains from the drill core yielding dates that lie within this range, there are outliers in two samples. Sample 21GC061A (N=11) includes one anomalously young ~6 Ma grain. Sample 21GC061C (N=7) had two young dates of 9 and 4 Ma.

Young grains in drill core samples were excluded from the sample average ages and will be investigated more closely using integrated AFT thermochronology.

AHe ages from detrital and bedrock samples collected from the Pilgrim Hot Springs thermal anomaly region range from 72 Ma to 0.5 Ma (Fig. 7). The youngest AHe single grain dates are from a detrital coarse sand sample collected at PHS in well PS-12-3 at the 1000 ft depth interval, which contains 11, 3, and 0.47 Ma dates, in addition to 22 and 24 Ma grains. The rest of the AHe single grain dates from PHS geothermal wells are generally older than 20 Ma, with a few grains in the 14 and 15 Ma range in well PS-12-2 at 1250 ft depth (Fig. 7).

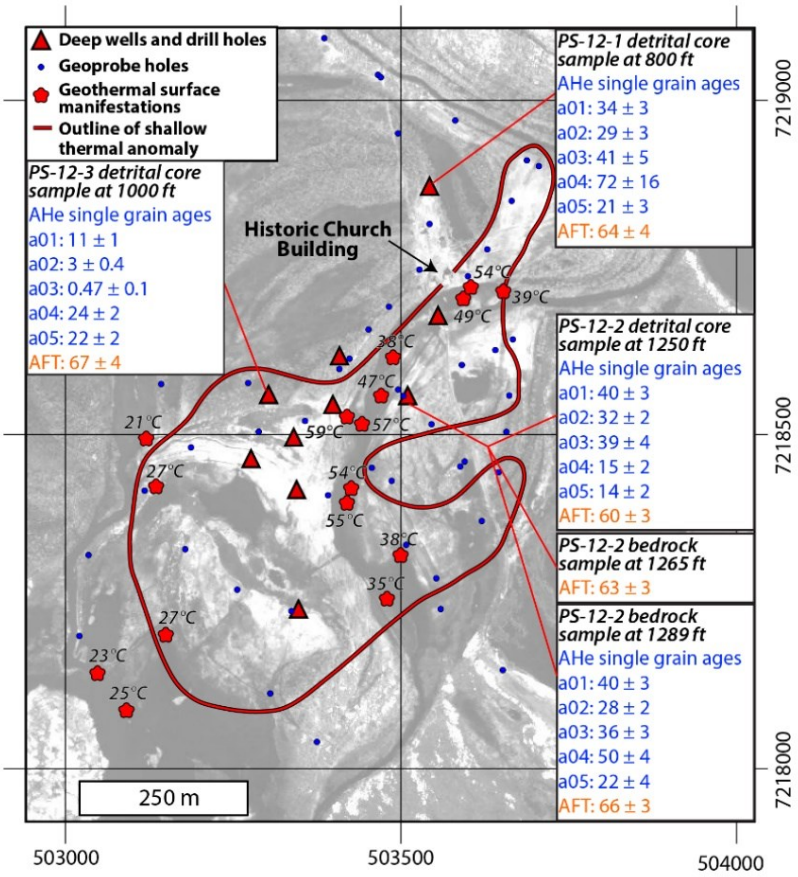

Figure 7: Map showing the location and approximate margin of the shallow Pilgrim Hot Springs thermal aquifer (red line), surface locations of geothermal springs (red stars), temperatures of thermal water (°C) measured at the surface, geoprobe locations (blue dots), and deep wells and drillholes (red triangles). Map location shown in Figure 3. The red boundary closely approximates the area where surface spring water and shallow geoprobe measurements exceed a temperature of 27°C. Detrital thermochronology results are shown for detrital samples collected in the identified wellbore and depth interval. AHe results are single age dates and AFT results are pooled ages (all ages in Ma). Figure modified from Benoit (2014a) and surface spring locations and temperatures from Haselwimmer et al. (2013).

3. DISCUSSION

North-south directed extension is accommodated along the active KFS and preexisting structures strongly influence the geometry and expression of faulting in the region. AHe results yield mostly 40-25 Ma dates along the portions of the KFS that have the most offset (both older offset and recent offset), with older dates (70-50 Ma) along the ends of the fault where there is less total displacement. The late Eocene-Oligocene AHe dates on fault-related basin formation have been connected to extension of this age in the Bering Sea region (McDannell et al., 2014; Dumitru et al., 1995) that formed basins offshore the Seward Peninsula on the north and south (Fig. 1) as discussed by Miller and Craig (this volume). Lack of consistent AHe dates younger than 25 Ma indicates that recent fault slip on the KFS has not exceeded more than ~ 2 km of the total offset necessary to exhume the AHe partial retention zone of 60-80°C if assuming a geothermal gradient of 25-30°C/km (e.g. Batir et al., 2016). The extent of slip on the KFS during different Cenozoic extensional events is inferred to be principally produced from late Eocene-Oligocene extension relative to minor modern extension.

Numerous samples collected along the trace of the KFS yield young AHe dates relative to background ages, including apatite grains from AP3, JC22-PS30, 21GC061A, and 21GC061C (Fig. 4). Young AHe dates indicate thermal disturbance of apatite and degassing of

radiogenic helium likely from circulation of hydrothermal fluids along the KFS. There are numerous thermal histories that could have produced the young AHe single grain ages, including: 1) complete thermal resetting and degassing of radiogenic He at temperatures above 80°C with subsequent cooling of samples through 60°C at the resultant date, and 2) partial degassing of He in apatite that could have occurred at various times (Eocene to recent), durations (days to millions of years), and temperatures (>60°C). Therefore, in a geothermal exploration context, young AHe single grain dates presented in this study from the trace of the KFS are not direct evidence for the presence of an active geothermal system. The combination of AFT and AHe data from the same sample can limit the number of acceptable cooling histories to constrain the timing and duration of thermal events (Ketcham, 2005; Donelick et al., 2005), and will be used in future work to delineate the role of hydrothermal fluids in the observed partially reset ages. Young AHe dates can help identify where to focus future detailed exploration of specific KFS segments having potential for active (or fossil) geothermal activity. The segments of the KFS near the Graphite Creek deposit and samples JC22-PS30 and AP3 show potential for hosting (or having hosted) a blind geothermal system.

The eastern segment of the KFS directly adjacent to PHS did not yield any young AHe dates. While the lack of young dates does not rule out the KFS as a possible structural control for PHS, we favor the conceptual model where a concealed fault that lies within the basin, the Pilgrim Springs fault (Fig. 3), is the primary structure controlling hydrothermal upwelling. GeoT multicomponent geothermometry yields 137°C equilibration estimates and confirms prior classical geothermometry estimates of >130°C. Young AHe dates from geothermal wells in the active outflow of the PHS geothermal system are similar in age to several samples collected from footwall rocks along the trace of the KFS, which is supporting evidence for blind geothermal activity along the KFS. Collectively, our results indicate that active fault systems of this region are the primary control for geothermal activity. There may be multiple geothermal resources present in this region and further exploration of these targets may ultimately result in a reliable source of energy for the nearby communities of the Seward Peninsula.

4. CONCLUSIONS

The KFS is an active, east-west striking normal fault accommodating modern north-south extension along preexisting structures. Preexisting structures important to the setting of PHS are related to extensional exhumation in the Late Cretaceous and Paleocene to Oligocene (Miller and Craig, this volume). Modern extension is young and has accommodated less than 2 km of total dip-slip motion along the KFS, and most of this slip is inferred to have occurred during the late Eocene-Oligocene. Several samples along the KFS yield young AHe dates, which is evidence for geothermal activity causing thermal diffusion of radiogenic helium. Areas along the KFS near young AHe dates are potential exploration targets for blind geothermal upwelling zones. Core samples of sedimentary rock from geothermal wells from PHS also yield young AHe dates, which are consistent with dates from footwall bedrock along the KFS. We attribute the primary structural control for PHS to be a blind fault within the Imuruk Basin and not the KFS. GeoT multicomponent geothermometry yields 137°C equilibration estimates for Pilgrim Hot Springs. The region along and north of the KFS may host structurally controlled blind geothermal systems likely capable of power production once successfully targeted.

5. ACKNOWLEDGEMENTS

Funding for this study was provided by a research grant from the TomKat Center for Sustainable Energy at Stanford University and by Zanskar Geothermal & Minerals, Inc. The authors are indebted to James Metcalf, Rebecca Flowers, Sabrina Kainz and others at the University of Colorado Boulder TRaIL lab for completing (U-Th)/He analyses. Thanks to Nic Spycher of the Lawrence Berkley National Laboratory for completing GeoT multicomponent geothermometry analyses. This paper was benefited by insightful discussions with Dick Benoit, Darrel Kaufman, Jason Briner, Travis Hudson, and Ronald Daanen. Graphite One, Inc. is thanked for granting access to core from their drilling operations at Graphite Creek. Monika Fleming and Joel Edwards provided support in the field for sample collection. Bering Air provided helicopter support.

REFERENCES

ACEP.: Pilgrim Hot Springs Geothermal Exploration 2010-2014, Final Report. Alaska Center for Energy and Power at the University of Alaska Fairbanks (2015), 842 p.

Allmendinger, R. W., Cardozo, N., and Fisher, D.: Structural geology algorithms: Vectors and tensors in structural geology: Cambridge University Press (2012).

Cardozo, N., and Allmendinger, R.W.: Spherical projections with OSX Stereonet: Computers & Geosciences, v. 51, (2013), p. 193 – 205, doi:10.1016/j.cageo.2012.07.021.

Amato, J. M. and Miller, E. L.: Geologic map and summary of the evolution of the Kigluaik Mountains gneiss dome, Seward Peninsula, Alaska, in, Gneiss Domes in Orogeny, edited by Whitney, D., Teyssier, C., Siddoway, C. S. Geological Society of America Special Paper 380, (2004), p. 295–306.

Amato, J. and Miller, E. L.: Orogenic mass transfer and orthogonal flow directions in extending continental crust: An example from the Cretaceous Kigluaik gneiss dome, Seward Peninsula, Alaska, Geological Society of America Special Paper 360, 133-14, (2002).

Amato, J.M., Wright, J., Gans, P.B., and Miller, E.L.: Magmatically induced metamorphism and deformation in the Kigluaik gneiss dome, Seward Peninsula, Alaska, Tectonics, 13, (1994), 515–527.

Batir, J.F., Blackwell, D.D., and Richards, M.C.: Heat flow and temperature-depth curves throughout Alaska: finding regions for future geothermal exploration, Journal of Geophysics and Engineering, 13, (2016), p. 366-377. doi:10.1088/1742-2132/13/3/366

Benoit, D., Pike, C., and Holdmann, G.: The Pilgrim thermal anomaly, Geothermal Resources Council Transactions, Vol. 38, (2014a).

Benoit, D., Pike, C., and Holdmann, G.: Fluid-entry temperatures, depths, and water chemistry at Pilgrim Hot Springs, Alaska, Geothermal Resources Council Transactions, Vol. 38, (2014b).

Berger, A., Egli, D., Glotzbach, C., Valla, P.G., Pettke, T., Herwegh, M.: Apatite low-temperature chronometry and microstructures across a hydrothermally active fault zone. Chemical Geology, v. 588, (2022), 120633, https://doi.org/10.1016/j.chemgeo.2021.120633

Berman, M.: Energy costs and rural Alaska out-migration. (2017), http://hdl.handle.net/11122/7814.

Briner, J.P., Tulenko, J.P., Kaufman, D.S., Young, N.E., Baichtal, J.F. and Lesnek, A.: The last deglaciation of Alaska. Cuadernos de investigación geográfica: Geographical Research Letters, v. 43, (2017), p.429-448.

Calvert, A.T., Gans, P.B., and Amato, J.M.: Diapiric ascent and cooling of a sillimanite gneiss dome revealed by $^{40}Ar/^{39}Ar$ thermochronology: the Kigluaik Mountains, Seward Peninsula, Alaska. In: Ring, U., Brandon, M. T., Lister, G. S. & Willet, S. D. (eds) Exhumation Processes: Normal Faulting, Ductile Flow and Erosion. Geological Society, London, Special Publications, 154, (1999), 205-232.

Curewitz, D. and Karson, J.A.: Structural settings of hydrothermal outflow: Fracture permeability maintained by fault propagation and interaction: Journal of Volcanology and Geothermal Research, v. 79, (1997), p. 149–168, doi: 10.1016/S0377-0273(97)00027-9.

Donelick, R.A., O'Sullivan, P.B., Ketcham, R.A.: Apatite Fission-Track Analysis. Reviews in Mineralogy and Geochemistry; 58 (1), (2005), p. 49–94. doi: https://doi.org/10.2138/rmg.2005.58.3

Dumitru, T.A., Miller, E.L., O'Sullivan, P.B., Amato, J.M., Hannula, K.A., Calvert, A.T., and Gans, P.B.: Cretaceous to Recent extension in the Bering Strait region, Alaska: Tectonics, v. 14, (1995), no. 3, p. 549–563. http://doi.org/10.1029/95TC00206

Farley, K.A.: Helium diffusion from apatite: general behavior as illustrated by Durango fluorapatite. Journal of Geophysical Research. vol. 105, (2000), p. 2903 – 2914.

Flowers, R.M., Zeitler, P.K., Danišík, M., Reiners, P.W., Gautheron, C., Ketcham, R.A., Metcalf, J.R., Stockli, D.F., Enkelmann, E., Brown, R.W.: (U-Th)/He chronology: Part 1. Data, uncertainty, and reporting. GSA Bulletin; 135 (1-2), (2022A), 104–136. doi: https://doi.org/10.1130/B36266.1

Flowers, R.M., Ketcham, R.A., Enkelmann, E., Gautheron, C., Reiners, P.W., Metcalf, J.R., Danišík, M., Stockli, D.F., and Brown, R.W.: (U-Th)/He chronology: Part 2. Considerations for evaluating, integrating, and interpreting conventional individual aliquot data: Geological Society of America Bulletin, Special Volume on Reporting and Interpretation of Geochronologic Data, v. 134, (2022b), https://doi.org/10.1130/B36268.1.

Ginster, U., Reiners, P.W., Nasdala, L., and Chanmuang, N.C.: Annealing kinetics of radiation damage in zircon: Geochimica et Cosmochimica Acta, v. 249, (2019), p. 225–246, https://doi.org/10.1016/j.gca.2019.01.033.

Glen, J.M.G., McPhee, D.K., Bedrosian, P.A.: Geophysical investigations of the geologic and hydrothermal framework of the Pilgrim Springs geothermal area, Alaska, Proceedings, Thirty-Ninth Workshop of Geothermal Reservoir Engineering Stanford University, Stanford, California, February 24–26 2014, 9 p.

Gorynski, K. E., Walker, J. D., Stockli, D. F., and Sabin, A.: Apatite (U–Th)/He thermochronometry as an innovative geothermal exploration tool: A case study from the southern Wassuk Range, Nevada, Journal of Volcanology and Geothermal Research, v. 270, (2014), p. 99–114, https://doi.org/10.1016/j.jvolgeores.2013.11.018.

Guenthner, W.R., Reiners, P.W., Ketcham, R.A., Nasdala, L., and Giester, G.: Helium diffusion in natural zircon: Radiation damage, anisotropy, and the interpretation of zircon (U-TH)/He thermochronology: American Journal of Science, v. 313, (2013), p. 145–198, https://doi.org/10.2475/03.2013.01.

Hamilton, T.D., Reed, K.M., and Thorsen, R.M.: Glaciation in Alaska. Alaska Geological Society, Anchorage. Alaska. (1986).

Haselwimmer, C., Prakash, A., Holdmann, G.: Quantifying the heat flux and outflow rate of hot springs using airborne thermal imagery: Case study from Pilgrim Hot Springs, Alaska, Remote Sensing of Environment, 136, (2013), p. 37-46.

Hudson, T., and Plafker, G.: Kigluaik and Bendeleben faults, Seward Peninsula, in Johnson, K.M., ed., The United States Geological Survey in Alaska—Accomplishments during 1988: U.S. Geological Survey Circular 772-B, (1978), p. 47–50.

Johnson, J.E., Flowers, R.M., Baird, G.B. and Mahan, K.H.: "Inverted" zircon and apatite (U–Th)/He dates from the Front Range, Colorado: High-damage zircon as a low-temperature (< 50°C) thermochronometer. *Earth and Planetary Science Letters*, *466*, (2017), pp.80-90.

Kaufman, D.S.: Surficial geologic map of the Solomon, Bendeleben, and southern part of the Kotzebue quadrangles, western Alaska: U.S. Geological Survey Miscellaneous Field Studies Map MF-1838-A, (1986), 1 sheet, scale 1:250,000.

Ketcham, R.A.: Forward and inverse modeling of low-temperature thermochronometry data: Reviews in Mineralogy and Geochemistry, v. 58, (2005), p. 275–314, https://doi.org/10.2138/rmg.2005.58.11.\

Koehler, R.D., Carver, G.A., and Alaska Seismic Hazards Safety Commission.: Active faults and seismic hazards in Alaska: Alaska Division of Geological & Geophysical Surveys Miscellaneous Publication 160, (2018), 59p. http://doi.org/10.14509/29705.

Kolker, A.M.: Geologic setting of the central Alaskan hot springs belt: Implications for geothermal resource capacity and sustainable energy production, Ph. D. Thesis, University Alaska, Fairbanks, (2008), 203p.

Kunze, J.F., and Lofgren, B.E.: Pilgrim Springs, Alaska, geothermal; resource exploration, drilling, and testing: Geothermal Resources Council S Transactions, v. 7, (1983), p. 301–304.

Liss, S.A., and Motyka, R.J.: Pilgrim Springs KGRA, Seward Peninsula, Alaska: Assessment of fluid geochemistry, Geothermal Resources Council Transactions, v. 18, (1994), p. 213–219.

Lofgren, B. E., Woodward –Clyde.: Geothermal energy development at Pilgrim Springs, Alaska, Phase II: results of drilling testing and resource confirmation April 15, Report Submitted to State of Alaska Division of Energy and Power Development, (1983), 62 p.

Louis, S., Luijendijk, E., Dunkl, I., Person, M.: Episodic fluid flow in an active fault. Geology, 47 (10), (2019), 938–942. doi: https://doi.org/10.1130/G46254.1

MacNamee, A.F.: Thermochronometric investigation of structural evolution and geothermal systems in extensional settings, Dixie Valley, Nevada, (MSthesis). Austin, Texas: University of Texas, Austin. (2015). http://hdl.handle.net/2152/32600

McDannell, K. T., Toro, J., Hourigan, J. K., and Harris, D.: Thermochronologic constraints on Late Cretaceous to Cenozoic exhumation of the Bendeleben Mountains, Seward Peninsula, Alaska, Geochem. Geophys. Geosyst., 15, (2014), 4009–4023, doi:10.1002/2014GC005424.

Milesi, G., Soliva, R., Moni´e, P., Münch, P., Bellanger, M., Bruguier, O., Bonno, M., Taillefer, A., Mayolle, S.: Mapping a geothermal anomaly using apatite (U/ Th)/He thermochronology in the Tˆet fault damage zone, eastern Pyrenees, France. Terra Nova, v.31, (2019), p. 569–576. https://doi.org/10.1111/ter.12429.

Miller, E.L., and Craig, J.W.: Regional Tectonic setting of Pilgrim Hot Springs, Seward Peninsula, Alaska, Fourty-Ninth Workshop on Geothermal Reservoir Engineering, Stanford University, Stanford, CA (2024).

Miller, E. L., Calvert, A. T., Little, T. A.: Strain-collapsed metamorphic isograds in a sillimanite gneiss dome, Seward Peninsula, Alaska, Geology v. 20 (6), (1992), p. 487-490.

Miller, T. P.: Geothermal resources of Alaska, in Plafker, G., and Berg, H. C., eds., The Geology of Alaska: Boulder, Colorado, Geological Society of America, The Geology of North America, v. G-1, (1994).

Miller, T. P.: Distribution and chemical analyses of thermal springs in Alaska, U. S. Geological Survey Open-file Map 570, scale 1:2,500,000, (1973).

Miller, J. K., Prakash, A., Daanen, R., Haselwimmer, C., Whalen, M., Benoit, D., Cumming, W., Clark, A. C., Mager, M., and Holdmann, G.: Geologic model of the geothermal anomaly at Pilgrim Hot Springs, Seward Peninsula, Alaska, PROCEEDINGS, Thirty-Eighth Workshop on Geothermal Reservoir Engineering, Stanford University, Stanford, CA (2013a).

Miller, J. K., Haselwimmer, C., and Prakash, A.: Investigating low temperature hydrothermal alteration in drill cuttings from Pilgrim Hot Springs, Alaska, using a suite of low cost analytical techniques, Geothermal Resources Council Transactions, Vol. 37, (2013b), p. 989 – 995.

Motyka, R.J., Forbes, R.B., and Moorman, M.: Geochemistry of Pilgrim Springs thermal waters, in Turner, D.L., and Forbes, R.B. eds., A geological and geophysical study of the geothermal energy potential of Pilgrim Springs, Alaska, Fairbanks, University of Alaska Geophysical Institute Report UAG R–271, (1980), p. 43–52.

Porter, C., Howat, I., Noh, M., Husby, E., Khuvis, S., Danish, E., Tomko, K., Gardiner, J., Negrete, A., Yadav, B., Klassen, J., Kelleher, C., Cloutier, M., Bakker, J., Enos, J., Arnold, G., Bauer, G., Morin, P.: ArcticDEM – Strips, Version 4.1: Harvard Dataverse, V1, (2022). https://doi.org/10.7910/DVN/C98DVS

Reiners, P.W., Ehlers, T.A., and Zeitler, P.K.: Past, present, and future of thermochronology. "Reviews in Mineralogy and Geochemistry 58, no. 1, (2005), p. 1-18.

Richards, M., and Blackwell, D.: A difficult search: Why Basin and Range systems are hard to find: Geothermal Resources Council Bulletin, v. 31, (2002), p. 143-146.

Rizzo, A.L., Robidoux, P., Aiuppa, A. and Di Piazza, A.: $^{3}He/^{4}He$ Signature of Magmatic Fluids from Telica (Nicaragua) and Baru (Panama) Volcanoes, Central American Volcanic Arc. *Applied Sciences*, *12*(9), (2022), p. 4241.

Spycher, N., Peiffer, L., Saldi, G., Sonnenthal, E., Reed, M.H., Kennedy, B.M.: Integrated multicomponent solute geothermometry. Geothermics, v. 51, (2014), p. 113–123.

Tagami, T., and O'Sullivan, P.B.: Fundamentals of fission-track thermochronology: Reviews in Mineralogy and Geochemistry, v. 58, (2005), p. 19–47, https://doi.org/10.2138/rmg.2005.58.2.

Till, A. B., Dumoulin, J.A., Werdon, M.B., Bleick, H. A.: Bedrock Geologic Map of the Seward Peninsula, Alaska, and Accompanying Conodont Data, U.S. Department of the Interior, U. S. Geological Survey, (2011).

Turner, D.L. and Swanson, S.E.: Continental rifting—A new tectonic model for the central Seward Peninsula. Geothermal

reconnaissance survey of the central Seward Peninsula, Alaska: University of Alaska, Geophysical Institute, Report prepared for the Division of Geothermal Energy of the US Department of Energy, Report, 284, (1981), pp.7-36.

Tulenko, J. P., Briner, J. P., Young, N E., Schaefer, J. M.: The last deglaciation of Alaska and a new benchmark ^{10}Be moraine chronology from the western Alaska Range, Quaternary Science Reviews, Volume 287, (2022), 107549, ISSN 0277-3791, https://doi.org/10.1016/j.quascirev.2022.107549.

Wescott, E., and Turner, D.L., Geothermal reconnaissance survey of the central Seward Peninsula, Alaska: Alaska Geophysical Institute Report UAG-R284, (1981).

Young, N.E., Briner, J.P., Schaefer, J., Zimmerman, S., Finkel, R.C.: Early Younger Dryas glacier culmination in southern Alaska: Implications for North Atlantic climate change during the last deglaciation: Geology, v. 47, (2019), p. 550-554.